

An Evaluation of the SCSN Moment Tensor Solutions: Robustness of the M_w Magnitude Scale, Style of Faulting, and Automation of the Method

by John F. Clinton,* Egill Hauksson, and Kalpesh Solanki

Abstract We have generated moment tensor solutions and moment magnitudes (M_w) for >1700 earthquakes of local magnitude (M_L) >3.0 that occurred from September 1999 to November 2005 in southern California. The method is running as an automated real-time component of the Southern California Seismic Network (SCSN), with solutions available within 12 min of event nucleation. For local events, the method can reliably obtain good-quality solutions for M_w with $M_L >3.5$, and for the moment tensor for events with $M_L >4.0$. The method uses the 1D Time-Domain INverse Code (TDMT_INV) software package (Dreger, 2003). The Green's functions have been predetermined for various velocity profiles in southern California, which are used in the inversion of observed three-component broadband waveforms (10–100 sec), using data from at least four stations. Moment tensor solutions have an assigned quality factor dependent on the number of stations in the inversion, and the goodness of fit between synthetic and observed data. If a minimum quality factor is attained, the M_L or M_w is 5.0 or greater, and if the event is in the southern California reporting regions, the M_w will be the official SCSN/CISN magnitude.

The M_w from the high-quality solutions determined from our method generally correlate very well with reviewed M_L , except in regions at the perimeter of the network. The M_w reported here indicates the SCSN M_L systematically underestimates the magnitude in the Mexicali region of Baja California, Mono Lakes area, Coso region, and the Brawley seismic zone, and overestimates the magnitude in the Coastal Ranges.

Comparisons of the moment tensors determined using this model are made with Harvard Centroid Moment Tensors generated for larger earthquakes in the California region, and recent 3D models for events in the Los Angeles region, with excellent correlation.

Most of the earthquakes with good-quality solutions exhibit strike-slip faulting, in particular, along the major late Quaternary strike-slip faults. Thrust faulting on east-west-striking planes is observed along the southern edge of the Transverse Ranges, while northwest-striking thrust faulting is observed in the Coastal Ranges. Normal faulting is most common in Baja California and southern Sierra Nevada including the western Basin and Range region.

Poor-quality solutions with unreliable M_w are caused by excessive background noise in the waveforms. Small events ($M_L < 4.0$) can be affected by ambient noise or teleseisms, but larger events can also have unreliable solutions if they follow a recent large regional event.

Introduction

The dramatic increase in deployment of broadband seismic stations with real-time continuous telemetry has meant that moment tensor determination has become increasingly routine, and moment tensor solutions are now a common

product of many seismic networks across the globe. The moment tensor, with an associated moment magnitude, M_w , is typically determined by an inversion of three-component broadband seismograms from several stations. Depending on the inversion technique, seismograms from regional and teleseismic distances can be used. Because the time required for the complete broadband waveform to arrive at a station

*Present address: Swiss Seismological Service (SED), Department of Geophysics, Swiss Federal Institute of Technology (ETH), Zürich.

is far shorter for regional events, regional schemes are best suited for rapid moment tensor determination. They also can be used to identify moment magnitudes for smaller events with local magnitudes as low as M_L 3.5. Regional moment tensor solutions still require complete broadband waveforms, and so require complete time series recovery before the inversion can commence. Though this means the M_w cannot be computed as rapidly as with other magnitudes, an automated moment tensor solution can provide an improved estimate of magnitude that is less prone to saturation than magnitude scales based on limited frequency bandwidths (Kanamori, 1977; Heaton *et al.*, 1986), though essentially the two scales should theoretically be equal (Deichmann, 2006). In addition, the moment tensor solution also documents the fault characteristics and constrains the depth, giving insight into the tectonic setting of the event. This information can be vital to the emergency response after a strong earthquake.

Currently near-real-time global moment tensor solutions are provided by the Harvard Centroid Moment Tensor (CMT) Project (www.seismology.harvard.edu/projects/CMT/) (Dziewonski *et al.*, 1981; Dziewonski and Woodhouse, 1983), the U.S. Geological Survey (USGS) National Earthquake Information Center (NEIC) (<http://neic.usgs.gov/>) (Sipkin, 1982, 1994), and the Earthquake Research Institute (ERI) in Japan (Kawakatsu, 1995). Regional moment tensor solutions are currently computed in near-real time using a variety of methods (Dreger and Helmberger, 1993; Romanowicz *et al.*, 1993; Nabelek and Xia, 1995; Randall *et al.*, 1994; Thio and Kanamori, 1995; Ammon *et al.*, 1998). Pasyanos and Romanowicz (1996), Fukuyama *et al.* (1998), Bernardi *et al.* (2004), and Rueda and Mezcua (2005) document the real-time implementation of some of these methods.

The Southern California Seismic Network (SCSN) (www.scsn.org), a component of the California Integrated Seismic Network (CISN), has recently added an automated procedure to determine the regional moment tensor and moment magnitude for all local events greater than M 3.0. The SCSN network operates over 180 broadband stations with distribution across southern California (Hauksson *et al.*, 2001), and monitors additional broadband data from the Berkeley Digital Seismic Network (BDSN, <http://seismo.berkeley.edu/bdsn/>) and the Anza Seismic Network (ANZA, <http://eqinfo.ucsd.edu/projects/anza/>). These stations create one of the most dense and well distributed regional broadband networks in the world (see Fig. 1). The automated solution is designed to take advantage of the network density to search for an optimal solution from all stations as fast as possible.

Each moment tensor solution has an assigned quality factor dependent on the number of stations in the inversion and the goodness of fit between synthetic and observed data. Dependent on the quality, the M_w and moment tensor may be automatically distributed to the general community through e-mail, USGS Recent Earthquake web pages, and CISNDisplay. In general, for events with $M_L > 4$, a high-

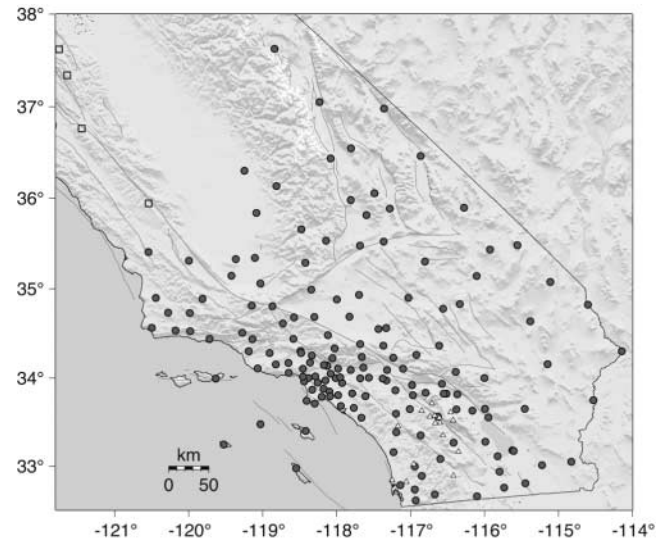


Figure 1. Broadband sensors in southern California available for use in the real-time moment tensor solution, November 2005. SCSN broadband station locations are indicated by circles; triangles are ANZA stations; squares indicate the subset of BDSN broadband stations available to SCSN.

quality moment tensor solution is publicly available within 10 min of the event initiation. All solutions populate the searchable archive hosted by Southern California Earthquake Data Center (SCEDC; www.data.scec.org/). A web interface has been developed for duty seismologists to evaluate, modify if necessary, and redistribute the automatic solution. If a minimum quality factor is attained and if the event is in the southern California reporting regions, the M_w will be the official SCSN/CISN magnitude.

The real-time algorithm has been applied to all regional events with $M_L > 3.5$, and local events with $M_L > 3.0$, since September 1999, from the SCSN catalog stored at the SCEDC. For local events, the method can reliably obtain good quality solutions for M_w with $M_L > 3.5$, and for the moment tensor for events with $M_L > 4.0$. Further, the method provides backup solutions for large events outside of the SCSN reporting region, such as in northern California or Baja California.

This study describes the development and implementation of the automated solution, and describes the moment tensor catalog developed using the operational real-time algorithm on all candidate events from the SCEDC catalog. The quality and robustness of the moment magnitudes are investigated by comparison with reviewed SCSN local magnitudes and independent moment magnitude estimates, with good correlation. The moment tensor solutions are also shown to be very similar to independent solutions for all large events, and, in general, the catalog solutions fit in with existing first-motion solutions, and the current interpretation of southern California tectonics.

The Automatic Inversion Process

The SCSN automated real-time moment tensor solution is based on the method developed by Doug Dreger and originally automated at Berkeley Seismological Laboratory (BSL) (<http://seismo.berkeley.edu/~dreger/mtindex.html>) (Pasyanos *et al.*, 1996; Dreger *et al.*, 1998). Similar versions of the algorithm are run by F-Net in Japan (<http://www.fnet.bosai.go.jp/>) (Fukuyama *et al.*, 1998; Fukuyama and Dreger, 2000) and by AEIC in Alaska (<http://www.giseis.alaska.edu/>).

The Inversion Scheme

The method uses three-component, low-frequency broadband waveform data from multiple stations at optimal azimuths and distances to estimate the point-source moment tensor, which is decomposed into a scalar seismic moment and the double-couple orientation parameters, strike, slip, and rake. Synthetic Green's functions, derived from the three fundamental faults (Jost and Hermann, 1989), are used as the basis functions. These fundamental fault synthetics are combined with various 1D velocity structures typical to southern, central, and offshore California (Dreger and Helmberger, 1993) to form a library of Green's functions that are used to match the observed waveforms. The Green's functions are calculated using the frequency wavenumber integration method (Saikia, 1994). The observed data, and the Green's functions used to match the solutions, are both filtered with corner periods dependent on magnitude of the event ($M_L < 4.2$, 10–50 sec; $4.2 < M_L < 5.5$, 20–50 sec; $M_L > 5.5$, 20–100 sec). This reflects the increased long-period energy generated by larger events.

The solution scheme is constrained to allow double-couple and compensated linear vector dipole (CLVD) components in the moment tensor solutions (Jost and Hermann, 1989). The isotropic component is forced to be zero.

The quality of a solution is determined by the goodness of the fit of synthetic data to the observed data. The variance reduction, VR , is a parametric measure of this fit, and is defined as

$$VR = 100 \times \left\{ 1 - \frac{\sum_{i=0}^N [\sqrt{x_i^2 - d_i^2}]}{\sum_{i=0}^N [\sqrt{x_i^2}]} \right\},$$

where x_i is observed waveform, d_i is synthetic waveform, N is number of samples in the record.

The variance reduction is calculated (1) for each station in the inversion (IVR) and (2) for the overall average of all the stations in any given inversion (OVR).

For each solution, the inversion is run with the point-source depth at various levels typical of southern California events (5, 8, 11, 15, 18, and 21 km). Inverting at shallower depths can give erroneous solutions for the moment tensor, and deeper events are not realistic for events in southern California. The optimal solution depth is chosen as the so-

lution with the maximum overall variance reduction. The location of the event is not allowed to vary; event latitude and longitude are constrained to be the SCSN location.

Real-Time Solution

The goal of the automated scheme is to rapidly find the best-quality solution available for an event given the observed waveforms. This requires selecting stations that are well distributed azimuthally, with good signal-to-noise ratios. The steps involved are: (1) gather all available data and perform initial quality control; (2) select stations for the initial inversion by choosing waveforms from different azimuths at optimal distance for best signal-to-noise ratio; (3) perform inversion; (4) if the inversion results do not satisfy the desired quality, reject stations with the poorest waveform fits, and select new stations subject to the constraint of maximizing the available azimuthal distribution; repeat steps (2) and (3) with remaining stations; (5) if the station list is exhausted without reaching a solution of the desired quality, the quality required is relaxed and steps (2) to (4) are repeated.

The automatic solution algorithm is triggered whenever a local event with $M_L > 3.0$, or a regional event with $M_L > 3.5$, is identified by the SCSN real-time system. Once the algorithm is triggered, three-component 1 sample/sec $LH?$ high-gain broadband velocity data are collected for all candidate stations from the SCSN wavepool. The station list comprises over 180 sites (all SCSN stations [network code CI], all ANZA stations [AZ], and selected BDSN stations [BK]). Strong-motion data are currently not used in the solution. As the high pass for large events is 100 sec, a record length of 360 sec is selected to improve the stability of the record after bandpass filtering. The 360-sec window includes 60 sec of pre-event initiation data, and 300 sec of data post-event initiation. This means the inversion procedure does not begin until 5 min after the event initiates.

Selected data must (1) be from high-gain broadband sensors with corner periods of at least 100 sec, (2) be from stations between 45 and 700 km of the epicenter, and (3) have maximum amplitudes of any component below 80% of the clipping level of the broadband instruments (0.8×2^{23} counts, or ~ 0.8 cm/sec). In a given inversion, each selected station is from a different azimuthal sector defined about the epicenter. The initial station selection within each sector is the station closest to an epicentral distance of 60 km.

The minimum sensor corner of 100 sec limits the dataset to stations with CMG-3T, CMG3-ESP, STS-1, and STS-2 sensors only, and excludes the 40-sec CMG-40T sensors. This is because, after deconvolving the instrument response from the 40-sec sensor, the noise near 100 sec is very high. As only sensors with corners greater than 100 sec are used, the data do not require instrument deconvolution beyond division by the flat velocity gain. The distance criteria ensure selected waveforms have near-field and regional waveform characteristics, which are included in the modeled Green's functions.

The clipping criteria have been applied as recent research indicates broadband sensors can have a nonlinear response significantly short of their expected clip level (Clinton, 2004). Once data are retrieved from the wavepool, only data that satisfy these constraints is considered for the inversion.

Initially the region is divided into six sectors about the event epicenter. If one of the sectors does not contain at least one qualifying station (which may happen if most of the sector is ocean), the region will be divided into additional sectors, until six populated sectors are available. The inversion is then performed using the station closest to 60 km from each populated sector.

For each inversion, the overall variance reduction (OVR) and individual variance reduction (IVR) for each station are recorded. The real-time algorithm assigns a quality value to each inversion result, dependent on the OVR, IVR, and the number of stations in the inversion. The three distinct solution qualities are:

Quality A. The best solution is Quality A (six stations, OVR >60%). The moment tensor and M_w are publicly distributed without review. To obtain the best solution possible, initially the algorithm searches for a solution with OVR >85%; Quality A+. Figure 2 presents the waveform fits for a Quality A+ solution. Quality A solutions have moment tensor and M_w values that are independent of station selection if the IVRs are also >60%.

If an inversion solution does not meet Quality A+, stations are rejected dependent on their IVR from the inversion. Stations with IVR below (OVR - 10%) or 75% are removed from the available station list and the station selection process is repeated.

If no combination of six stations can provide a solution that will satisfy all the Quality A+ criteria, a Quality A solution will be searched for by using all initially available stations. In this case, the minimum OVR is 60%, and the minimum IVR is (OVR - 10%) or 50%.

Quality A solutions can be found for most events above M_L 4.0.

Quality B. If a Quality A solution cannot be obtained, the search for a Quality B solution automatically ensues, with relaxed criteria for the number of stations and OVR (four stations, OVR > 40%). Solutions of this nature have a robust M_w (with regard to station selection), fit for immediate distribution, though the moment tensor often varies with selected stations and is not considered stable enough for distribution.

For the Quality B solution, station selection follows the same method as described in the Quality A search; stations are chosen from, in this case, four azimuthal sectors. All available stations will have been included in at least one inversion in the attempt to find an A solution, and so a maximum IVR is known for each station. In this case, instead of

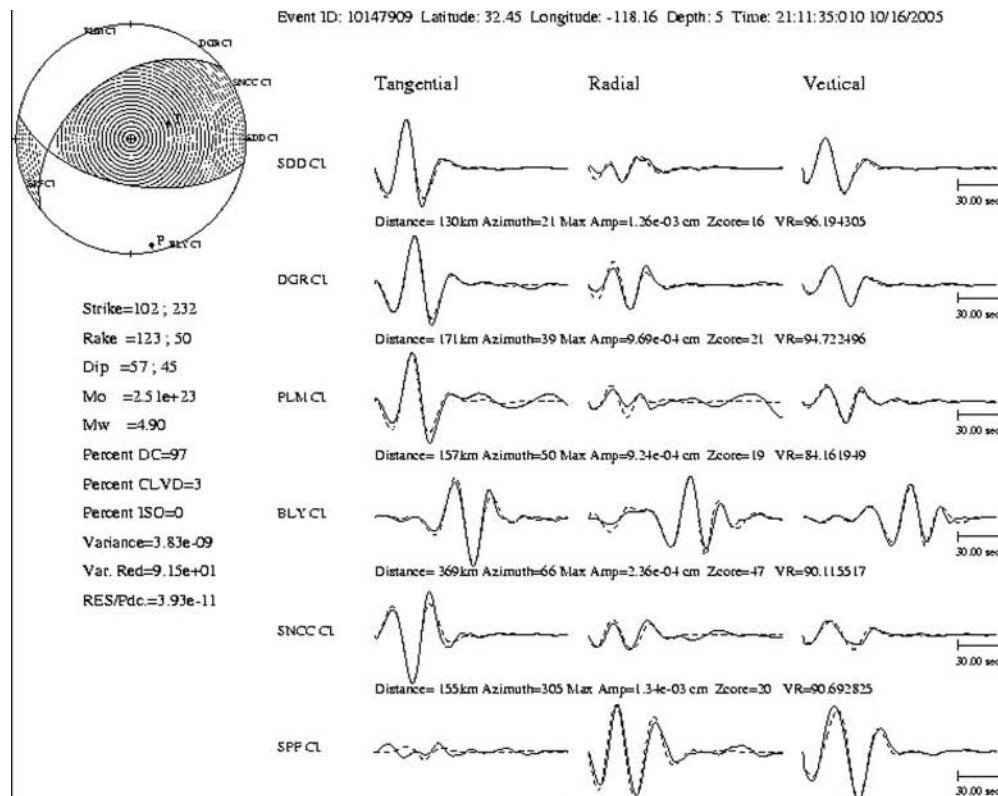


Figure 2. Typical waveform fits for a Quality A solution.

choosing stations in order of their proximity to the optimal distance, the station with the maximum IVR in each quadrant is selected. If a Quality B solution is attainable with the stations available, this speeds up the time taken to reach a solution. Following a failed attempt this solution, stations are rejected if the IVR is below 25% or (OVR – 15%).

Quality C. If no solution can be found that satisfies the Quality B criteria, a Quality C solution is immediately calculated using the four stations with highest peak IVR as determined from the Quality A and B inversion attempts. Station selection for this quality type does not take into account azimuthal distribution.

A Quality C solution does not typically have stable M_w or moment tensor, and there is no automatic distribution of the solution, though the solution does populate the SCEDC database.

The solution resulting from the successful inversion for Quality A, B, or C, is the real-time solution. It is automatically e-mailed to SCSN operators. All events that trigger the algorithm will have at least a Quality C solution. In many cases, especially if the event magnitude is small, and/or the event is located far from the center of the network, the automatic algorithm cannot obtain a Quality A or B solution. In such cases, it is likely the signal to noise is simply too low in the frequency of interest for all the stations in the network. In some cases, such as for large or interesting earthquakes, or if an event narrowly misses out on a Quality A or B solution, the duty seismologist may want to manually select and deselect stations, and repeat the inversion to try to improve the solution. In these cases, stations can be manually selected using an interactive website, by-passing the automatic station rejections.

For Quality A and B solutions, real-time and web-modified solutions are distributed to the public via e-mail lists, USGS Recent Earthquakes web pages, CISNDisplay, and the SCEDC. The SCEDC hosts a website with permanent archive which queries the SCSN moment tensor database (http://www.data.scec.org/catalog_search/CMTsearch.php).

The SCSN Catalog of Moment Tensor Solutions: 1999 to Present

Continuous data have been recorded by SCSN and archived at the SCEDC since late September 1999 (an effort initially in response to the Hector Mine earthquake). The solution is run on all local events with $M_L > 3.0$, and $M_L > 3.5$ for regional earthquakes, in the SCEDC catalog since this date. All events with solutions (>1700 events by November 2005) are presented in Figure 3. Each focal mechanism is color-coded for Quality A, B, and C. Larger events are typically of Quality A.

Figure 4 shows M_w versus reviewed SCSN M_L for each quality bin for the dataset. The 281 Quality A events exhibit similar values for M_L and M_w —almost all events have under

a 0.5 magnitude unit difference. Several larger events differ by more than 0.3 magnitude units, and it will be subsequently shown these are real differences, as independent M_w solutions replicate these differences. The average difference in the magnitudes for the Quality A solutions (Fig. 4a) is effectively zero over the entire catalog. For the 212 Quality B solutions (Fig. 4b), M_w is on average only 0.06 greater than M_L . The standard deviation on both solutions is about 0.2 magnitude units. The very small average difference between the two scales demonstrates there is no systematic magnitude bias in the moment magnitude calculation.

In Figure 5 the similarity of depths from the real-time solution and the M_w solution are investigated. The depth from the M_w algorithm does not correlate well with the real-time solution depth, regardless of solution quality. This is because for a significant number of events, the variance reduction is not sensitive to the event depth, and so is not well constrained. Nonetheless, the M_w depths derived from waveform modeling, and M_L depths derived from phase picks, usually agree fairly well where both are well constrained. However, if there are no nearby stations and, in particular, the M_L depths are poorly constrained, the depths may differ significantly. In such cases, the M_w depths are usually preferred because surface-reflected phases can provide improved depth constraints (Zhu and Helmberger, 1996).

The 1999 dataset is not complete; only partial time sequences starting from September are available for a limited number of stations. The M_w 7.1 Hector Mine mainshock clips all available broadband stations, so no solution is possible. The aftershock sequence from this event was so robust there are many more events from the subsequent 4 months of the year than from any other year in the catalog. Unfortunately, the occurrence of many events very closely spaced in time, recording on recently clipped sensors, means there are numerous events with $M_L > 4$ with low-quality solutions and many events have inflated magnitudes. The relatively limited SCSN station density at the time also contributes to poor solutions. Figures 4c and 4d illustrate this point. Since 1999, the only events with $M_L > 4.5$ with Quality C solutions are two events that occurred >300 km offshore (Fig. 3), with very poor azimuthal constraint by the network. Similarly, the 2003 San Simeon sequence following the 22 December M_w 6.5 mainshock contains many Quality C solutions with elevated M_w above M_L 3.5.

The San Simeon and the 28 September 2004 M_w 6.0 Parkfield earthquake are the two largest of the 20 regional events with $M_L > 5$ that have occurred since 1999. All these moderate events have Quality A solutions. The percentage of Quality A solutions above M_L 4.0 has remained high since 1999.

Regional Variations in the Relationship between M_w and M_L

The regional distribution of events showing a large discrepancy between M_L and M_w for Quality A and B is sum-

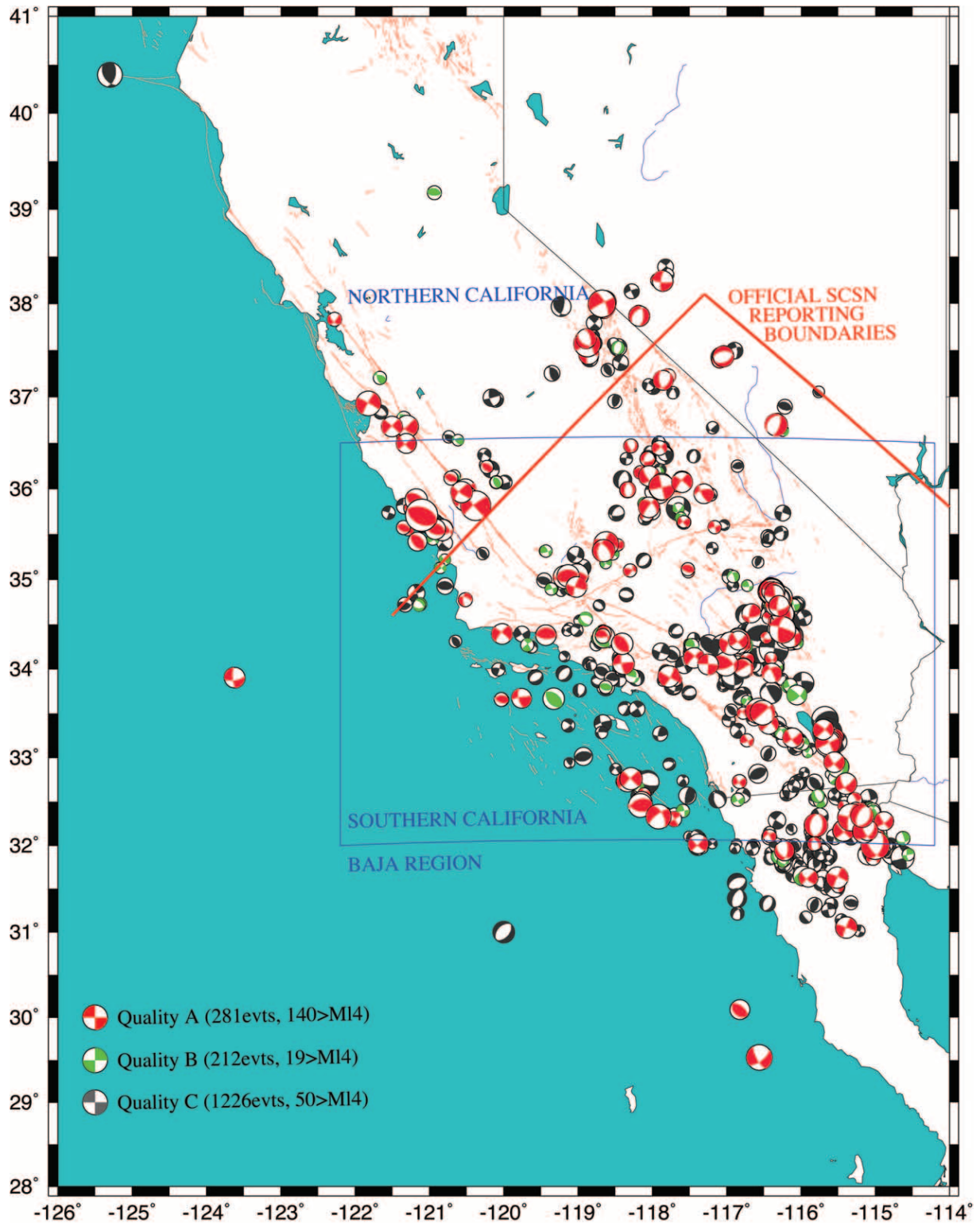


Figure 3. Locations and focal mechanisms from the entire catalog (September 1999 to November 2005). The box labeled “Southern California” indicates the region analyzed in Figures 8–10. Note: all events with $M_w < 4.0$ are artificially reduced in diameter.

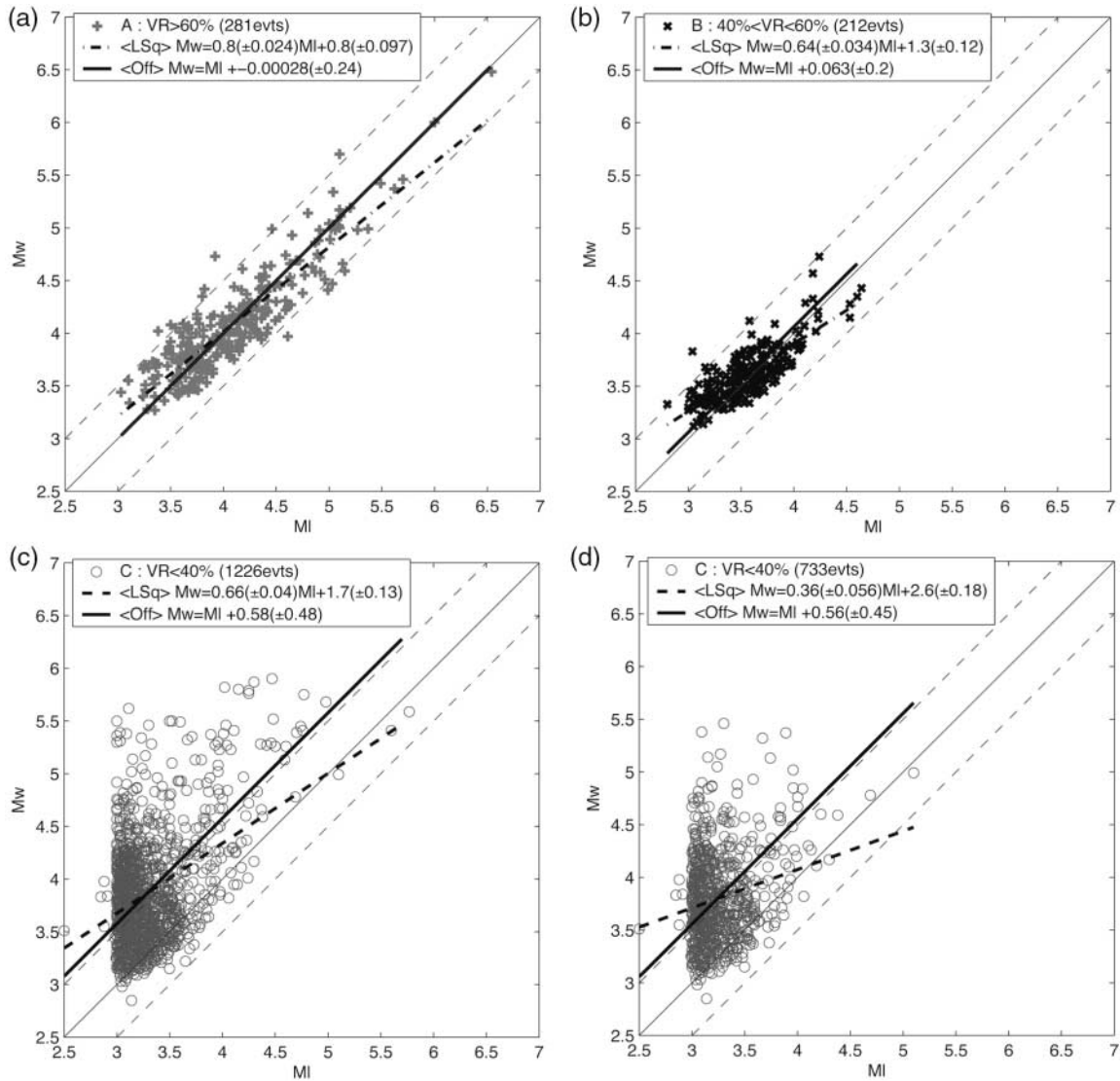


Figure 4. Comparisons for reviewed SCSN M_L and SCSN catalog M_w solutions for the entire catalog (September 1999 to November 2005). Data are presented for each Quality type. (a) Quality A solutions; (b) Quality B solutions; (c) Quality C solutions; (d) Quality C solutions 2000–2005. Solid thin lines are $M_w = M_L$, dashed thin lines are $M_w = M_L \pm 0.5$. The least-squares solution and the average magnitude offset (with standard deviations for each variable) are indicated in each subfigure. The average magnitude offset between M_L and M_w for Quality A solutions (a) is effectively zero and is about 0.06 magnitude unit for Quality B (Fig. 4b). Figure 4d shows only Quality C solutions from 2000 to November 2005, which removes the aftershock sequence from Hector Mine included in Figure 4c. The two Quality C solutions with $M_L > 4.5$ are from events over 300 km offshore (Fig. 3).

marized in Figure 6. Quality C events are omitted as they do not have reliable magnitude estimates. M_w solutions tend to be consistent with M_L throughout most of the network—Figure 4 shows on average there is effectively no difference between the magnitude scales for high Quality M_w solutions. Nevertheless, regions in Mono Lakes, Coso, the Brawley Seismic Zone and Baja California have clusters of events with $M_w > M_L$. The regions near Coso and Brawley experience earthquake swarming but minor events during swarms

do not have Quality A or B solutions. M_w is consistently below M_L in the Coastal Ranges—in particular the aftershock zone of San Simeon. The high M_w solutions near Hector Mine are due to noise during the robust aftershock sequence.

Figure 7 presents magnitude comparisons for all events occurring in each of the boxed regions in Figure 6 where there are clusters of magnitude discrepancy. Each region contains at least 20 high-quality solutions from at least M_L 3.2 to M_L 5.0. Figure 7a–d all indicate there is a small sys-

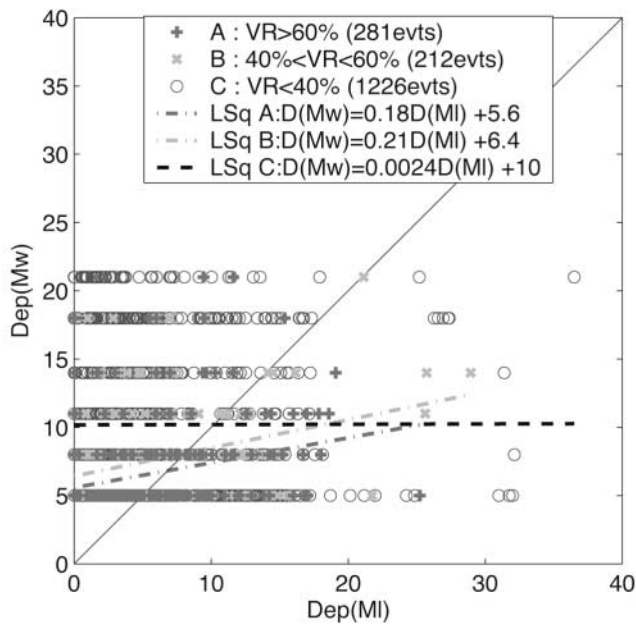


Figure 5. Depth comparisons for reviewed SCSN M_L and SCSN moment tensor solutions, for the entire catalog (September 1999 to November 2005).

tematic underestimation of magnitude by the M_L . For the Quality A solutions, the largest discrepancy is in the Brawley region, which has a difference of 0.23 magnitude units. This is the only region with average offset being greater than the standard deviation. In all other cases, the average offset is below the standard deviation of at least 0.19 magnitude units. In the region comprising the Coastal Ranges and Parkfield (Fig. 7e), M_L appears to overestimate the magnitude, though the average is under 0.1 magnitude units, which is also under the standard deviation of 0.2. For all these regions, as well as the general southern California region represented in Figure 4, the least-squares fits all have a slope below 1, indicating small events can have overestimated M_w solutions. Previous studies of magnitude calibration in California (Gee *et al.*, 2003; Kanamori *et al.*, 1993) have also documented regions with systematic magnitude variation. In Switzerland, Braunmiller *et al.* (2005) have documented that larger variations exist between M_w and M_L determined within the same research group (0.2 magnitude units) and between M_L determined by differing regional agencies (up to 0.6 magnitude units). The M_L and M_w can differ geographically because they measure different frequency content of the seismic waves and because of effects such as frequency-dependent path attenuation (Erickson *et al.*, 2004).

Style of Faulting for Events in the Southern California Region

Figures 8, 9, and 10 show the locations, sizes, and mechanisms for events with predominantly strike-slip, thrust, and normal faulting, respectively. Only events within the south-

ern California geographical box indicated in Figure 3 are shown. This box includes parts of the northern California reporting region, which are analyzed as station density is still high (SCSN receives real-time data from numerous BDSN stations), and the 2003 San Simeon and 2004 Parkfield events occurred in the region.

All events with rake = $90^\circ \pm 45^\circ$ are defined as thrust events. Normal faulting is defined as all events with rake = $-90^\circ \pm 45^\circ$. All other events are defined to be strike-slip.

For the 1735 events in the catalog, 1026 (59%) are strike-slip, 351 (21%) are thrust, and 358 (20%) are normal. This same ratio is maintained for the events inside the geographical box shown in Figures 8, 9, and 10. For Quality A events inside the same geographical region, the percentage of strike-slip events rises to 73%, with only 17% and 10% of events exhibiting thrust and normal, respectively. The different qualities (A, B, or C) of focal mechanisms show almost identical spatial patterns. The waveform-based focal mechanisms reveal a similar picture of the style of faulting as previously obtained by Hardebeck and Hauksson (2001).

The majority of strike-slip faulting from 1999 to 2005 occurred along the major late Quaternary strike-slip faults, with much activity along the San Jacinto fault, the Elsinore fault, to the south of the San Andreas fault in Imperial Valley, and along strike-slip faults within the Continental Borderland. Numerous strike-slip events also occurred within the San Bernardino mountains and the Eastern California Shear Zone. The Coso-Ridgecrest region and parts of the Tehachapi mountains are also characterized by strike-slip faulting.

The thrust faulting events also occur scattered across southern California. The 2003 San Simeon earthquake sequence was characterized by northwest-striking thrust faulting, almost parallel to the strike of the San Andreas fault. In contrast, most of the thrust events located south of the Tehachapi mountains have occurred along planes forming high angles to the strike of the San Andreas fault. In particular, the Transverse Ranges are mostly dominated by east-west-striking thrust faulting. In contrast, both northeast- and northwest-striking thrust events occur within the Peninsular Ranges, which may be related to fault step-overs within the major strike-slip faults.

Normal faulting events have occurred at the southern tip of the Salton Sea in the Brawley seismic zone and south of the Imperial Valley in Baja California. These events are consistent with the rifting in the Salton Trough. Small events with normal faulting are also observed along the major strike-slip faults and in the southern edges of the Sierra Nevada, north of the Garlock Fault. Some of these normal events may be associated with geometrical complexity along the strike-slip faults. In regions where normal and thrust events almost coincide in location, the faulting occurs on orthogonal planes with, for instance, thrust faulting on east-west-striking planes and normal faulting on north-south planes.

The overall style of faulting is transtensional south of

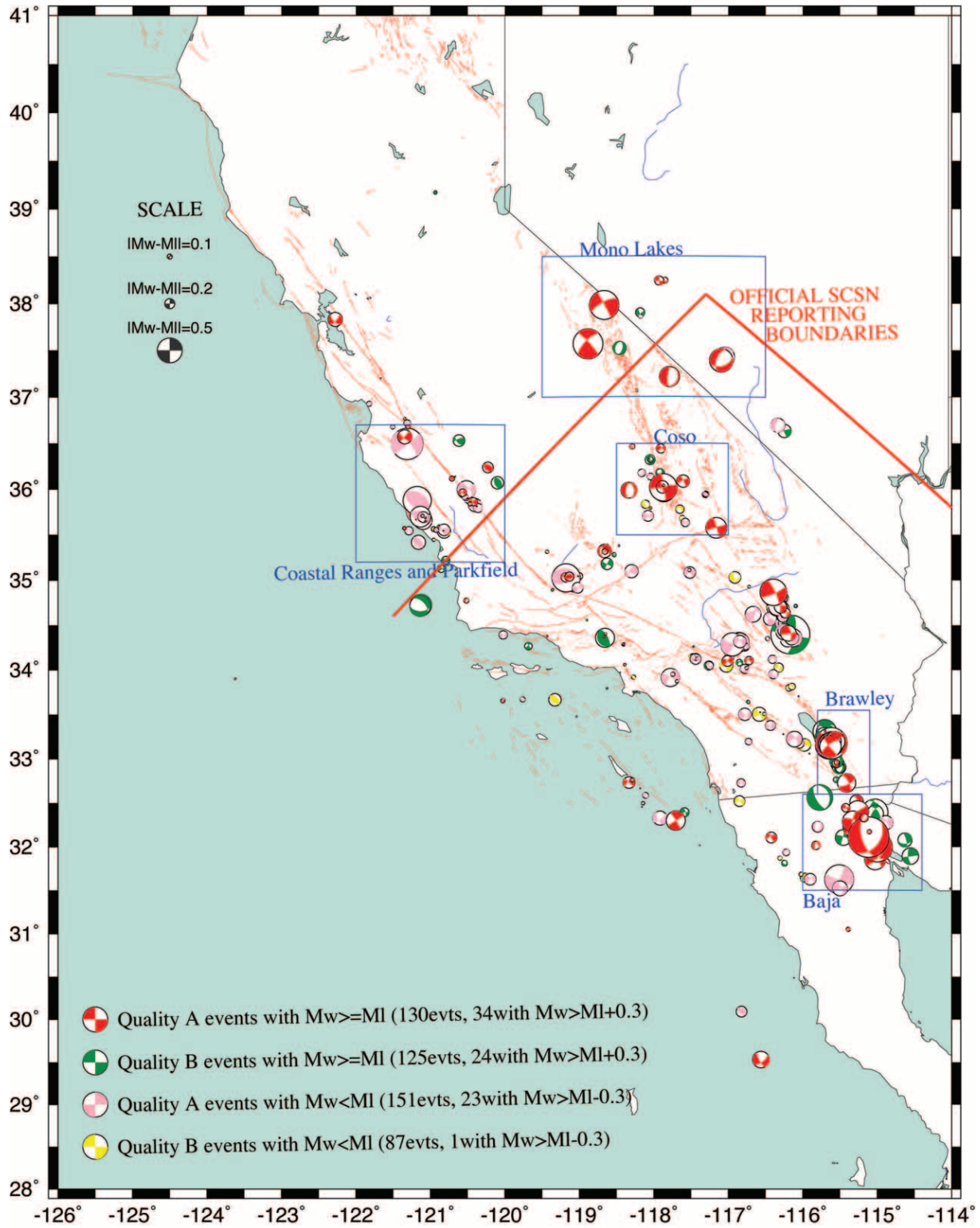


Figure 6. Geographical distribution of events exhibiting large differences between M_w and M_L for the entire catalog. Only events with Quality A and B are shown (Quality C does not have reliable magnitude). Dark-colored focal mechanisms indicate Quality A (red) and B (green) solutions with M_w greater than M_L . Light-colored focal mechanisms indicate Quality A (pink) and B (yellow) with M_w lower than M_L . The size of each focal mechanism is linearly scaled with $|M_w - M_L|$. M_w solutions tend to be consistent with M_L in most of the network, but regions in Mono Lakes, Coso, the Brawley Seismic zone, and Baja have clusters of events with $M_w > M_L$. M_w is consistently below M_L in the Coastal Ranges (in particular the aftershock zone of San Simeon).

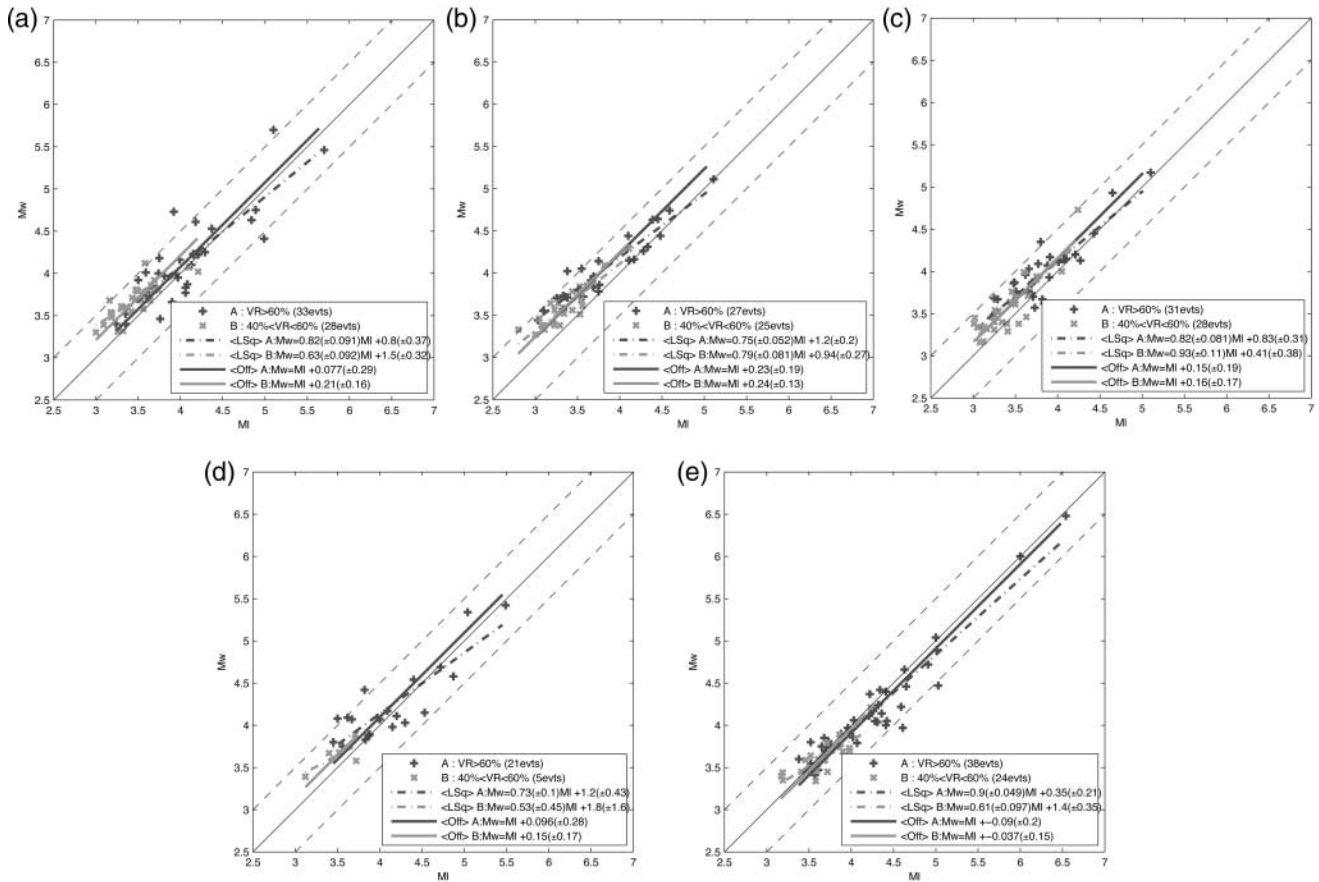


Figure 7. Magnitude comparisons for reviewed SCSN M_L and SCSN M_w solutions for each of the boxed geographical regions in Figure 6 (September 1999 to November 2005). (a) Baja Region; (b) Brawley Region; (c) Coso Region; (d) Mono Lakes Region; (e) Coastal Ranges and Parkfield. Thin solid lines are $M_w = M_L$, thin dashed lines are $M_w = M_L \pm 0.5$. Both the least-squares solution and magnitude offset (with standard deviation) are included for each quality type. Note each region has a small average magnitude offset, though none is greater than 0.25 magnitude units, and only Brawley has an offset greater than the standard deviation.

the Transverse Ranges and in the southern Sierra and Coso region. The style of faulting is transcompressional in the western Transverse Ranges, including the Los Angeles and Ventura basins, as well as along the Coastal Ranges in central California.

A Comparison of the SCSN Solution with Other Moment Tensor Solutions

The local magnitude scale saturates for events greater than M_w 6.5 (Heaton *et al.*, 1986). Additionally, as M_L is defined by the peak amplitude over a narrow bandwidth estimate of magnitude, and the M_w is determined from the fitting of full-length broadband waveforms, differences between M_L and M_w can be expected, especially for larger magnitude events. Accordingly, to establish calibration of the SCSN M_w implementation requires comparison with independent measures of M_w and the moment tensor.

The Harvard CMT catalog has solutions for 14 of the

events in the SCSN moment tensor catalog. Further, Liu *et al.* (2004) present moment tensor solutions from 3D inversions for three Los Angeles region events which also have other 3D solutions (based on methods described in Thio and Kanamori [1995] and Zhu and Helmberger [1996]). Data from these events are compared in Figures 11 and 12. The SCSN M_w and moment tensors are very similar to other moment tensor solutions over the broad geographical and magnitude ranges of the events in question. Braunmiller *et al.* (2005) demonstrate a similar variation in M_w exists between Harvard CMT and quick USGS moment tensor solutions.

Only in one of the 14 events is there a deviation in magnitude of more than 0.2 units between the SCSN M_w and other M_w solutions. Figure 12 shows there is far greater variation between the SCSN M_L and the other M_w solutions. All events that lie within the center of the reporting region have either nearly equivalent M_L and M_w or higher M_L . For most of the events located on the outskirts of the network aperture, the M_L is significantly lower than all the reported M_w

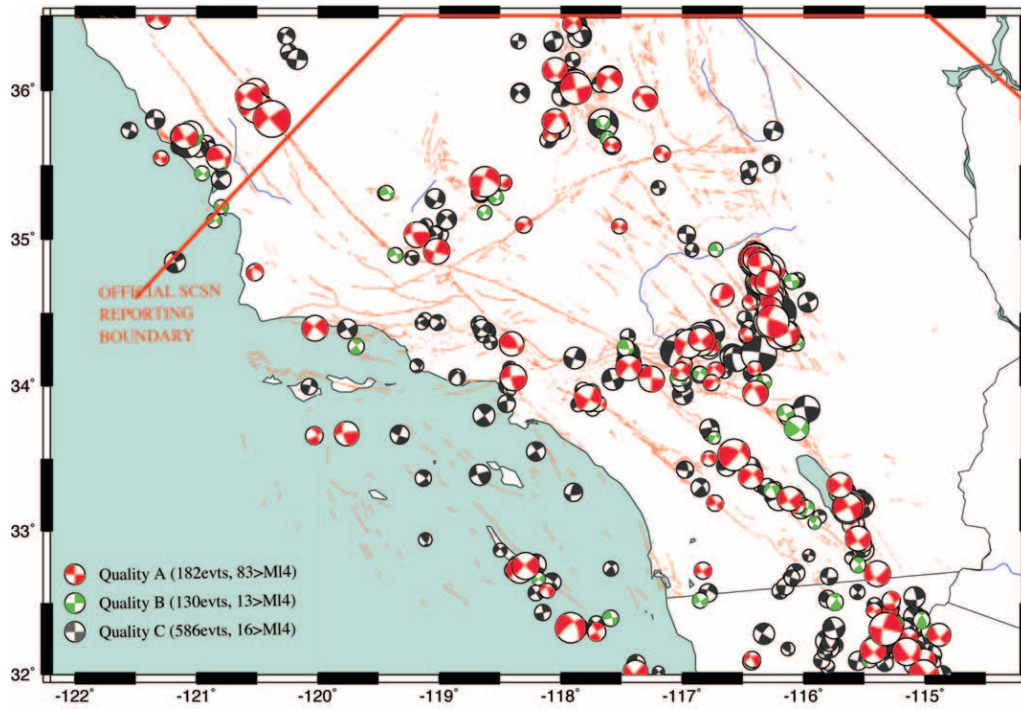


Figure 8. Locations and focal mechanisms for predominantly strike-slip events in the SCSN moment tensor catalog.

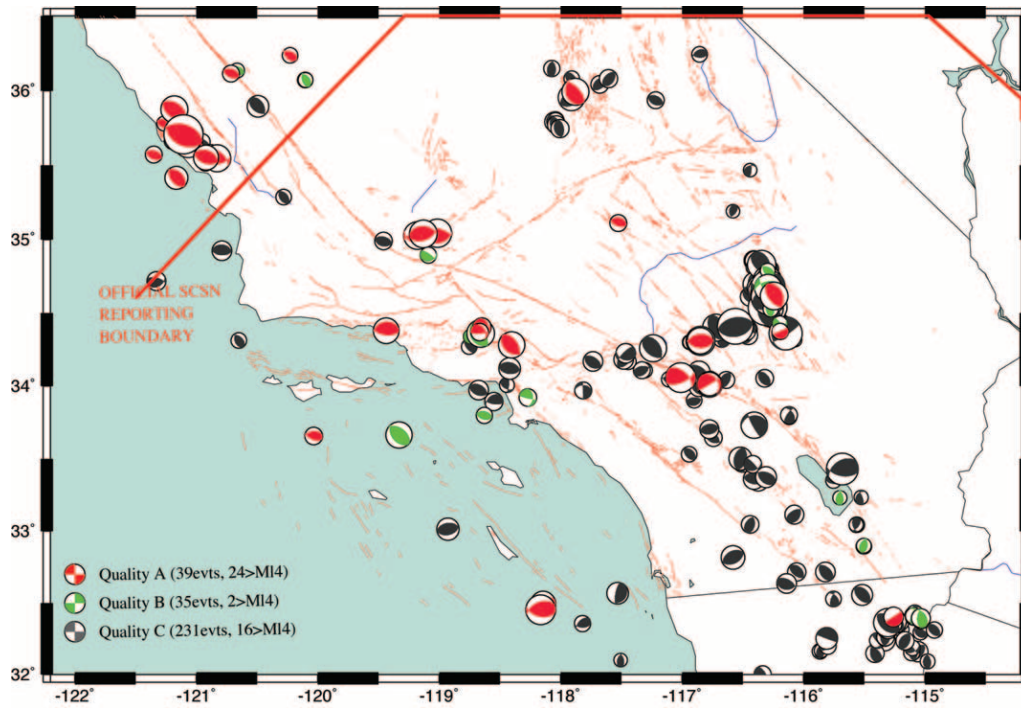


Figure 9. Locations and focal mechanisms for predominantly thrust events in the SCSN moment tensor catalog.

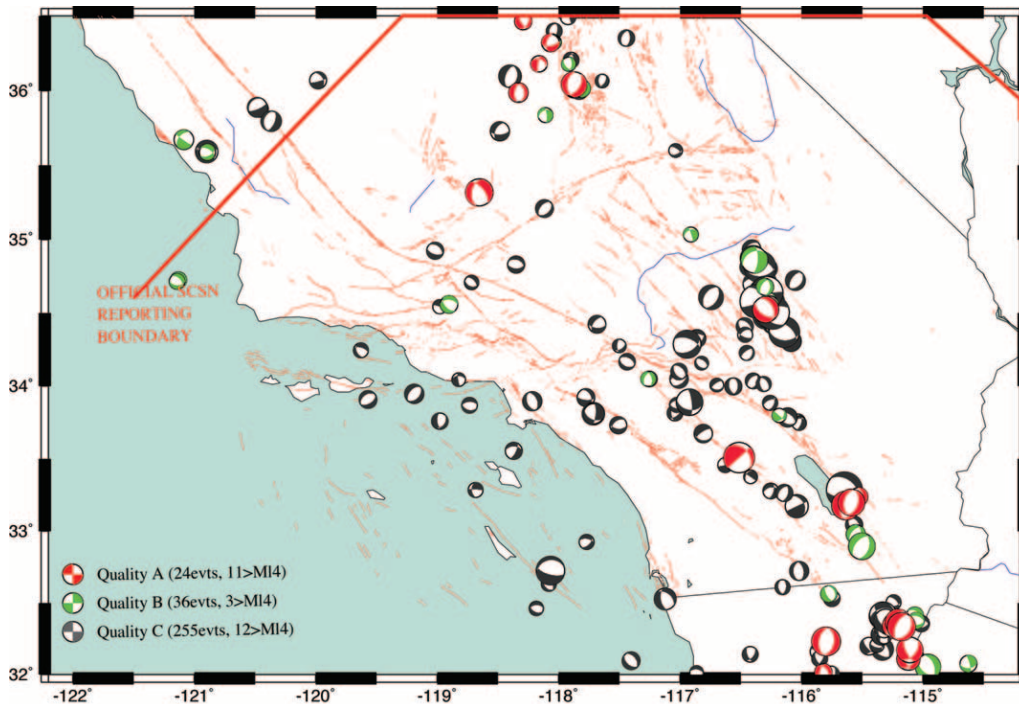


Figure 10. Locations and focal mechanisms for predominantly normal events in the SCSN moment tensor catalog.

(namely, events 1, 7, 9, and 11 on Fig. 12; only event 5 defies the trend). Thus it can be concluded (1) the deviations between M_w and M_L observed in the moment tensor catalog at large magnitudes (see Fig. 4) are true differences (and not an artifact of this M_w implementation), and (2) M_L is similar to or slightly higher than M_w for large events well constrained by the network. M_L appears to be systematically low for large events located outside the network aperture, except for earthquakes in the San Simeon aftershock region. This second conclusion is in agreement with the analysis of the overall dataset in the preceding section on regional variations.

Challenges with the SCSN Real-Time Moment Tensor Algorithm and Effects on the Robustness of M_w

Large Teleseisms

Teleseisms can introduce significant long-period energy into the local network, which can be well above the level produced by small and even moderate local events. This can cause erroneously large M_w with low OVR and a poor moment tensor solution. Figures 13 and 14 show an example from 15 July 2004, where a local M_L 3.0 is erroneously assigned a M_w 4.45 with $VR = 39\%$ due to incoming waveforms from a M_w 5.7 teleseism about 2000 km distant from southern California. This phenomenon is responsible for many of the M_w 4+ solutions with low VR in Figure 3.

To attempt to prevent modeling teleseismic noise, the

amount of time shift allowed in matching synthetics and observed data for each station is constrained. This time shift is measured by the ZCOR term, which is the shift (in seconds) required to obtain a peak cross-correlation between the synthetic and observed data. In Figure 2, the individual station ZCOR values only vary a small amount, proportional to distance. Additional scatter can be due to centroid location error, or path duration errors arising from simplified Green's functions. In Figure 14, there is large variation caused by modelling teleseismic noise, which dominates the event signal. A regression curve of ZCOR versus distance, r in kilometers, for all Quality A solutions produces the following relationship: $ZCOR_{\text{expected}} = 0.13r + 1.42$. Since November 2005, the real-time solution searches have the additional constraint: after an individual inversion, the expected station ZCOR is calculated. For any stations, if the difference between the observed and expected individual station ZCOR is greater than 9 sec, that station is automatically removed from the inversion.

Large Local and Regional Events

The M_w 7.1 Hector Mine event saturated all broadband stations available at the time of the event. A recurrence of this event should not clip the entire network in its current configuration; in addition to the greater number of SCSN stations, selected BDSN stations in northern California are also monitored by SCSN in real time.

In the event of the largest earthquake that can be expected in southern California, with $M_w > 8$, the SCSN al-

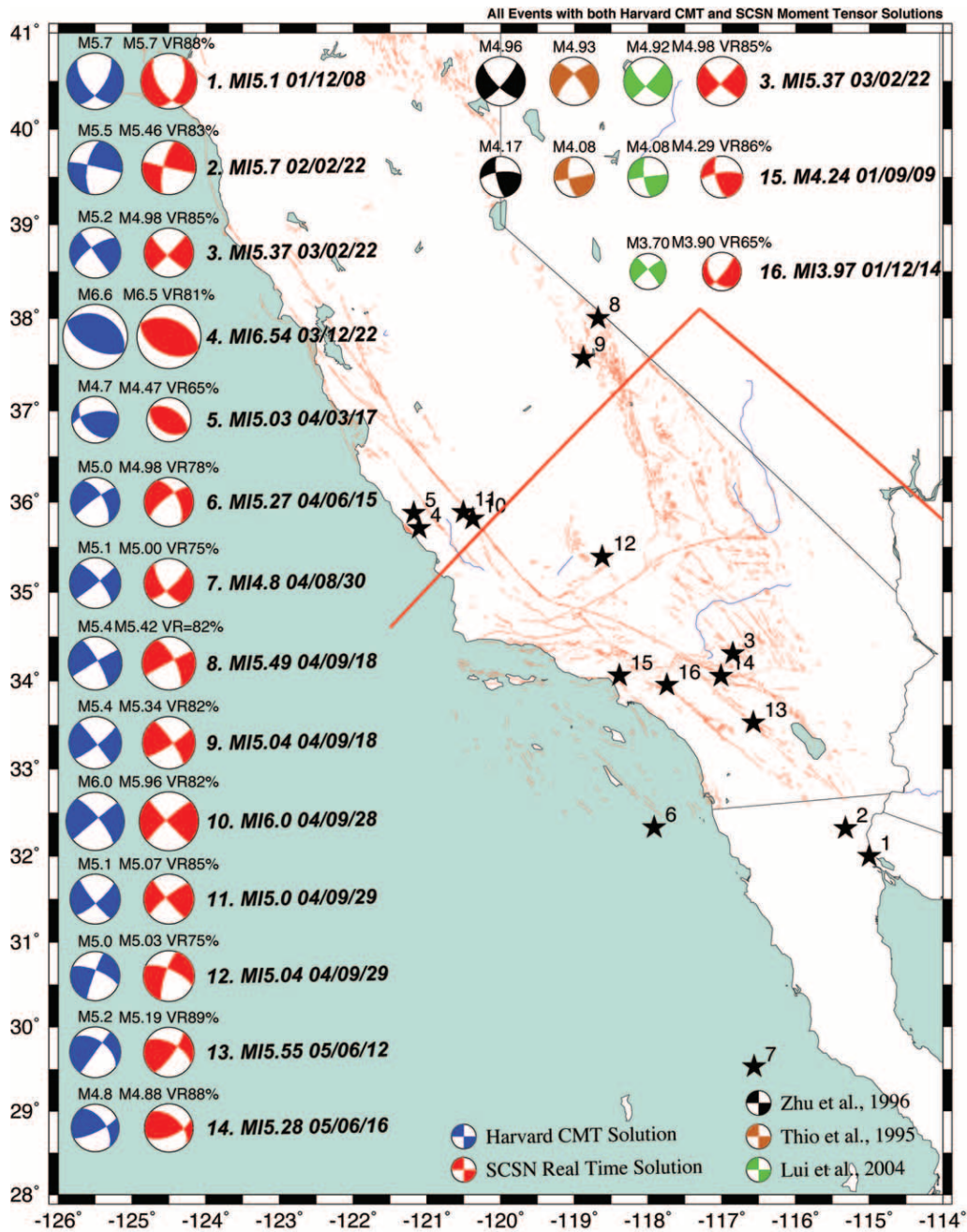


Figure 11. Location and focal mechanism map for regional events in California with independent M_w solutions in addition to the SCSN solution. A Harvard CMT solution is available for 14 events, and Liu *et al.* (2004) includes 3D solutions for three events using spectral element inversions as well as other techniques (Thio and Kanamori [1995] and Zhu and Helmberger [1996]).

gorithm may have difficulty obtaining a solution. The method assumes a point-source event, and all events larger than M_1 5.5 are modeled using data filtered between 20 sec and 100 sec with station distances up to 700 km. The point-source assumption in this case remains valid for events up to about M 7.0. For events larger than this, a valid point-source assumption would require stations at greater distances with bandpasses from 50 sec to 200 sec (Fukuyama and

Dreger, 2000). In any case, an event of magnitude greater than M 8.0 is likely to clip all broadband sensors out to many hundreds of kilometers distance (as seen in the M 8.3 Tokachi-Oki event [Clinton, 2004]). In these events, strong-motion data could be used because they will not clip, but this would require using Green's functions that (1) are defined in terms of velocity instead of displacement (as a double integration of accelerometer data to displacement pro-

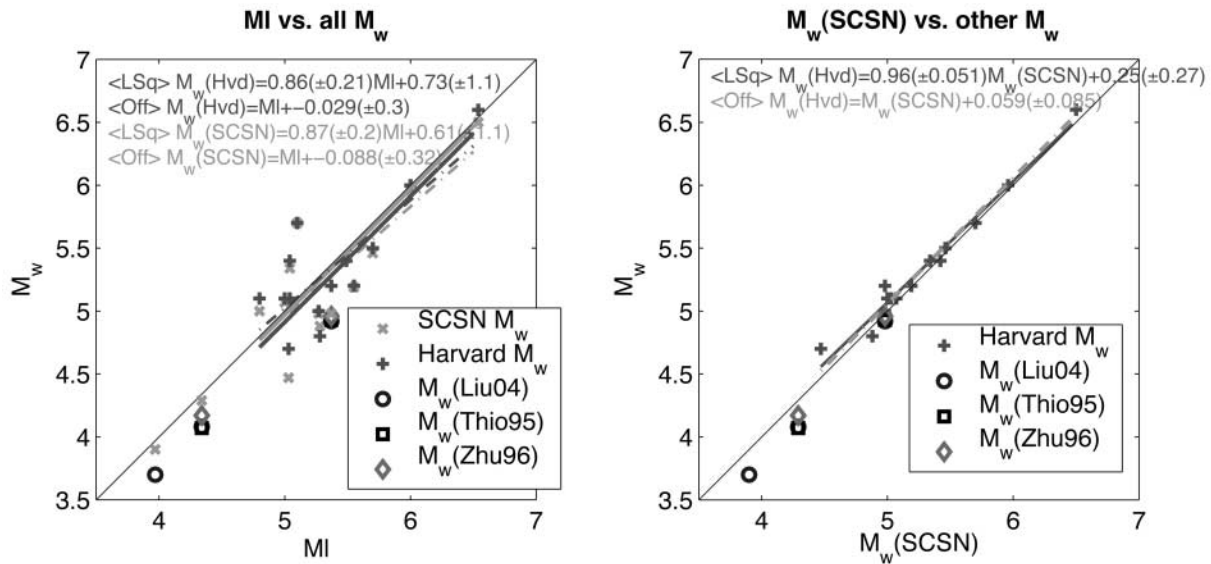


Figure 12. Comparison of various M_w solutions events shown in Figure 11. Note very little difference between M_w solutions, but larger variation between M_w and M_L . The four events with low M_L solutions all occur outside the SCSN network aperture. Both a least-squares best fit and magnitude offset (with standard deviations) are included for Harvard and SCSN M_w solutions.

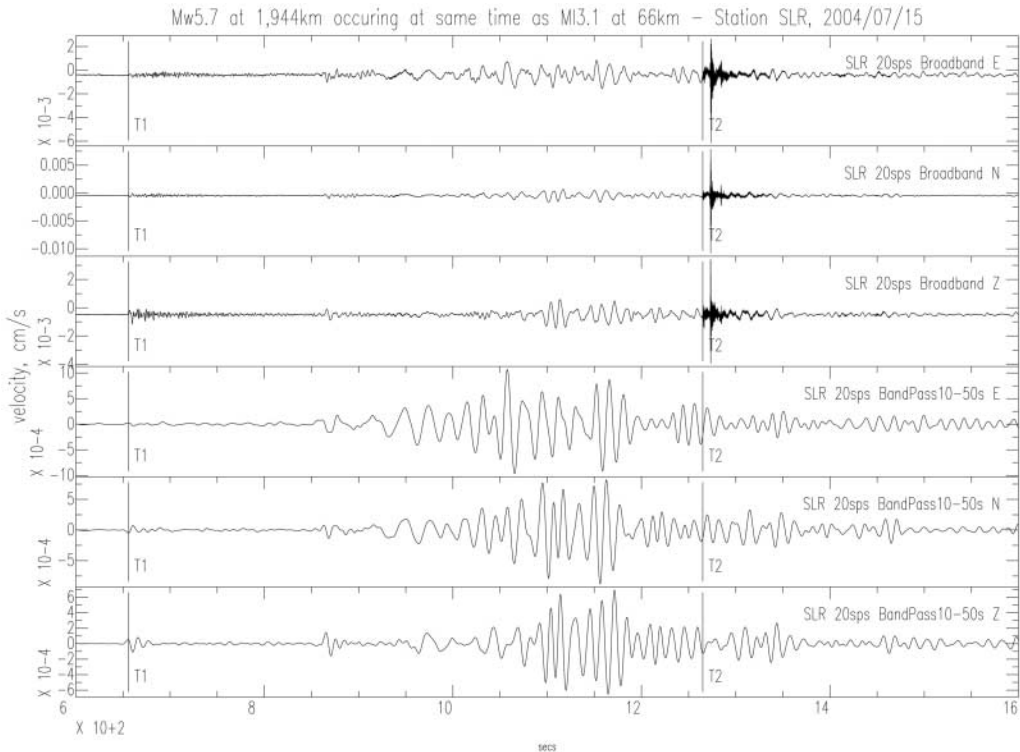


Figure 13. The effect of teleseismic waveforms on the inversion of small events. Three-component broadband data at station SLR; showing a M_w 5.7 at 1944 km (P -wave arrival marked as T1), with a local M_L 3.1 at 66 km (P -wave arrival at T2) occurring during the teleseism wavetrain. First three waveforms are E, N, Z raw unfiltered 20 samples/sec data; bottom three waveforms show the same data with a 10 to 50 sec filter. Note for the filtered data, the local event signal is lost in the teleseism wavetrain. The filter corners are the same as that applied in the SCSN moment tensor inversion for the local M_L 3.1 earthquake.

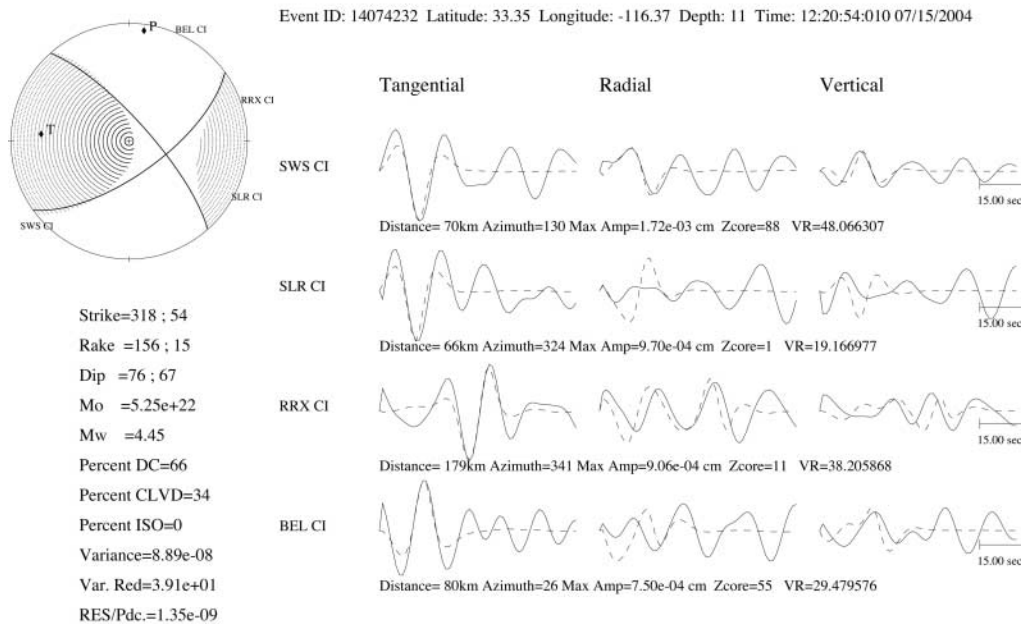


Figure 14. Automatic waveform fits for the local event in Figure 13. The M_L 3.1 is assigned a M_w 4.45 with 39% OVR, almost a Quality B solution. Note the ZCOR terms, a measure of the time shift required to optimally match observed and synthetic data, have much larger scatter than in Figure 2.

duces unstable noisy waveforms at very long periods); and (2) include near-field terms that are significant at many hundreds of kilometers distance for large events. As an alternative, to be able to constrain large-magnitude events in the future, SCSN plans to include some Advanced National Seismic System (ANSS) backbone stations from the midwest in the available list of monitored stations. The large epicentral distances at these stations will ensure the availability of broadband data which remain on-scale and do not violate the point-source approximation, though the waveforms would be at the limit of the regional waveform approximation.

Aftershock Sequences

The aftershock sequence of Hector Mine included numerous events within a few hours of the mainshock. These were assigned M_L solutions with a wide variation in magnitude, mostly below M_L 5. The moment tensor solution was unable to determine the magnitude of these events—all events within an hour of the mainshock had $M_w > 5.0$. The first Quality A solution after the event is a M_w 5.37 (M_L 5.63), 3 hours and 15 min after the mainshock. It appears the long-period motions from even large aftershocks during this period are drowned out by noise, not only from residual long-period energy from the mainshock, but more significantly, from increased sensor noise resulting from the recent violent sensor clipping during the mainshock. In Figure 15, M_w is observed to saturate at minimum M_w 4.2 for 3 hours after the event, with all but two events in this period having Quality C solutions. In the subsequent 5 days, the solutions are observed to improve, with most events above M_L 4.0

having Quality A or B solutions with good correlation between M_w and M_L .

The recent San Simeon and Parkfield events do not exhibit this same lack of resolution in the aftermath of the mainshock. Reasons for this include aftershock sequences not being as vigorous as those from the significantly larger Hector Mine event, and saturation of fewer broadband sensors (the area experiencing ground velocities above 1 cm/sec was reduced). Nevertheless, the increased density of stations may also be a factor in the improved performance.

Conclusions

Moment tensor and moment magnitudes, M_w , can be well determined in near-real time for almost all local southern California events with $M_L > 4$. Solutions are available within 12 min of an event trigger. A quality factor is assigned to each event, based on the number of stations used in the inversion, and the overall VR of the fit of observed and modeled waveforms. Quality A is the best solution and, if obtained, is typically available within 10 min, with M_w and moment tensor automatically released to the public. If this solution cannot be found from the available station waveforms, a Quality B solution is subsequently searched for; if this is also unavailable, finally a Quality C solution is immediately determined. For Quality B, only M_w is automatically released, as the moment tensor solution may be unreliable. A Quality C solution is not released to the public, because it is likely to have both an unreliable M_w and moment tensor.

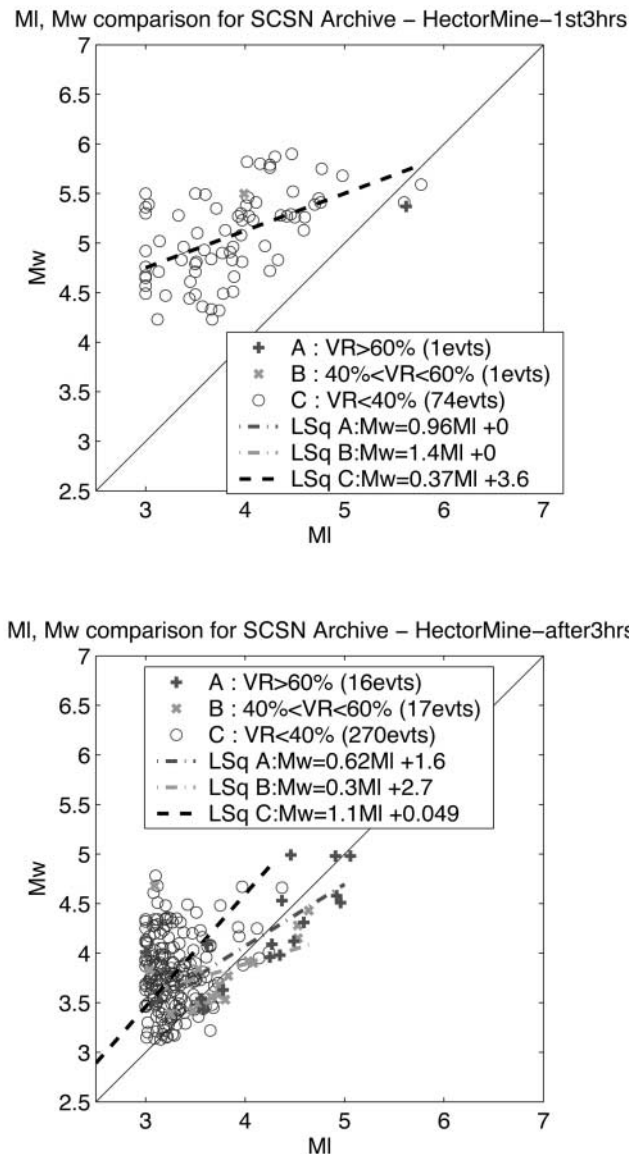


Figure 15. SCSN M_w solutions for events occurring within 3 hours of the Hector Mine mainshock, and all solutions over the subsequent 5 days. A dramatic improvement of the M_w solution occurs 3 hours after the mainshock.

The automatic solution can be modified using a web interface where the selected stations can be changed. For Quality A and B events within the SCSN reporting domain, solutions are distributed by e-mail and automatically created links, using QDDS, on CISNDisplay and the suite of USGS Recent Earthquakes web pages. For all solution types, a text e-mail, plot of VR versus depth, and the best depth waveform plot is available through SCSN/SCEDC. The SCEDC houses a searchable public archive of all moment tensor solutions from September 1999 (www.data.scec.org/).

The moment tensor is generally found to be stable ir-

respective of station selection for Quality A solutions, as long as individual station variance reduction is also high. Magnitude only is stable for Quality B solutions. Unless an event occurs during a robust aftershock sequence or during the passage of teleseismic waveforms through the network, Quality A solutions are obtained for most events with $M_L > 4.0$.

For the entire catalog of Quality A and B solutions, the average difference between M_L and M_w is negligible. The very small average difference between the two scales suggests there is no systematic magnitude bias in the moment magnitude calculation. Further, for events well constrained by the network, M_L is similar but systematically slightly higher than M_w . Conversely, for events occurring at or outside the perimeter of the network, in Baja California, the Brawley Seismic Zone, Coso and the Mono Lakes area, the M_L tends to be lower than the M_w . Events in the Coastal Ranges (including the San Simeon aftershock zone) and Parkfield regions toward the northwest of the network exhibit M_w solutions that appear to be systematically lower than the M_L . In all of these regions, the average difference varies 0.07–0.25 magnitude units, and the standard deviation is about 0.2 magnitude units. Saturation of the Richter Magnitude becomes significant for larger events. In all regions, the SCSN M_w and moment tensors are very similar to those observed by independent moment tensor solutions, including the Harvard CMT.

Moment tensor solutions in the catalog indicate the dominant type of faulting in southern California is strike slip, which is primarily distributed along the major late Quaternary strike-slip faults. For thrust faulting events, clusters of high-quality solutions are found for along the southern edge of the Transverse Ranges on east–west-striking planes, and in the Coastal Ranges along a northwest strike. Normal fault solutions are observed in Baja California south of the Imperial Valley and the southern Sierra Nevada.

Acknowledgments

Comments from the Associate Editor Jeanne Hardebeck, and an anonymous reviewer, greatly improved the manuscript. We thank Douglas Dreger, Lind Gee, Peggy Hellweg, and Pete Lombard from the Berkeley Seismological Laboratory for their discussions and advice. Georgia Cua also provided much feedback.

Moment Tensors are computed using the mtpackge v1.1 package developed by Douglas Dreger of the Berkeley Seismological Laboratory, and Green's functions were computed using the FKRRPROG software developed by Chandan Saikia of URS. Many of the figures were created with GMT (Wessel and Smith, 1998). Much of the manuscript was prepared while J.F.C. was at the University of Puerto Rico at Mayagüez (UPRM). The support of the Puerto Rico Strong Motion Program (PRSM) in the Civil Engineering Department at UPRM is gratefully appreciated. The SCSN is supported by NEHRP/USGS and ANSS through Cooperative Agreement 04HQAG0010, and California Office of Emergency Services through Contract 6028-2, and IRIS/USArray and IRIS/GSN through contacts 473 and 310; Contribution number 9147, Division of Geological and Planetary Sciences, California Institute of Technology, Pasadena.

References

- Ammon, C. J., R. B. Herrmann, C. A. Langston, and H. Benz (1998). Source parameters of the January 16, 1994 Wyoissing Hills, Pennsylvania earthquakes, *Seism. Res. Lett.* **69**, 261–269.
- Bernardi, F., J. Braunmiller, U. Kradolfer, and D. Giardini (2004). Automatic regional moment tensor inversion in the European-Mediterranean region, *Geophys. J. Int.* **157**, 703–716.
- Braunmiller, J., N. Deichmann, D. Giardini, and S. Wiemer and the SED Magnitude Working Group (2005). Homogeneous moment-magnitude calibration in Switzerland, *Bull. Seism. Soc. Am.* **95**, no. 1, 58–74.
- Clinton, J. F. (2004). Modern digital seismology—instrumentation, and small amplitude studies for the engineering world, *Ph.D. Thesis*, California Institute of Technology.
- Deichmann, N. (2006). Local magnitude, a moment revisited, *Bull. Seism. Soc. Am.* **96**, no. 4, 1267–1277.
- Dreger, D., R. Uhrhammer, M. Pasyanos, J. Franck, and B. Romanowicz (1998). Regional and far-regional earthquake locations and source parameters using sparse broadband networks: a test on the ridgecrest sequence, *Bull. Seism. Soc. Am.* **88**, no. 6, 1353–1362.
- Dreger, D. S. (2003). TDMT_INV: time domain seismic moment tensor inversion, in *International Handbook of Earthquake and Engineering Seismology*, W. H. K. Lee, H. Kanamori, P. C. Jennings, and C. Kisslinger (Editors), Vol. B, Academic Press, London, 1627 pp.
- Dreger, D. S., and D. V. Helmberger (1993). Determination of source parameters at regional distances with three-component sparse network data, *J. Geophys. Res.* **98**, no. B5, 8107–8126.
- Dziewonski, A., and J. Woodhouse (1983). An experiment in the systematic study of global seismicity: centroid-moment tensor solutions for 201 moderate and large earthquakes of 1981, *J. Geophys. Res.* **88**, 3247–3271.
- Dziewonski, A. M., T.-A. Chou, and J. Woodhouse (1981). Determination of earthquake source parameters from waveform data for studies of global and regional seismicity, *J. Geophys. Res.* **86**, 2825–2852.
- Erickson, D., D. E. McNamara, and H. M. Benz (2004). Frequency-dependent L_g Q within the continental United States, *Bull. Seism. Soc. Am.* **94**, no. 5, 1630–1643.
- Fukuyama, E., and D. S. Dreger (2000). Performance of an automated moment tensor determination system for the future “Tokai” earthquake, *Earth Planets Space* **52**, 383–392.
- Fukuyama, E., M. Ishida, D. S. Dreger, and H. Kawai (1998). Automated seismic moment tensor determination by using on-line broadband seismic waveforms, *Zisin* **51**, 149–156.
- Gee, L., D. Dreger, G. Wurman, Y. Gung, B. Uhrhammer, and B. Romanowicz (2003). A decade of regional moment tensor analysis at UC Berkeley, *EOS Trans. AGU* **84**, no. 46 (Fall Meeting Suppl.), abstract S52C-0148.
- Hardebeck, J., and E. Hauksson (2001). Crustal stress field in southern California and its implications for fault mechanics. *J. Geophys. Res.* **106**, no. 21, 21,859–21,882.
- Hauksson, E., P. Small, K. Hafner, R. Busby, R. Clayton, J. Goltz, T. Heaton, K. Hutton, H. Kanamori, J. Polet, D. Given, L. M. Jones, and D. Wald (2001). Southern California Seismic Network: Caltech/USGS Element of TriNet 1997–2001, *Seism. Res. Lett.* **72**, no. 6, 690–704.
- Heaton, T., F. Tajima, and A. Mori (1986). Estimating ground motions using recorded accelerograms, *Surv. Geophys.* **8**, no. 1, 25–83.
- Jost, M. L., and R. B. Hermann (1989). A student’s guide to and review of moment tensors, *Seism. Res. Lett.* **60**, 37–57.
- Kanamori, H. (1977). The energy release in great earthquakes, *J. Geophys. Res.* **82**, 2981–2987.
- Kanamori, H., J. Mori, E. Hauksson, T. Heaton, L. Hutton, and L. Jones (1993). Determination of earthquake energy release and ML using TERRAScope, *Bull. Seism. Soc. Am.* **83**, 330–346.
- Kawakatsu, H. (1995). Automated near-real-time CMT inversion. *Geophys. Res. Lett.* **22**, 2569–2572.
- Liu, Q., J. Polet, D. Komatitsch, and J. Tromp (2004). Spectral-element moment-tensor inversions for earthquakes in southern California, *Bull. Seism. Soc. Am.* **94**, no. 5, 1748–1761.
- Nabelek, J., and G. Xia (1995). Moment-tensor analysis using regional data: application to the march 25, 1993, Scotts Mills, Oregon, earthquake, *Geophys. Res. Lett.* **22**, 13–16.
- Pasyanos, M. E., D. S. Dreger, and B. Romanowicz (1996). Toward real-time estimation of regional moment tensors, *Bull. Seism. Soc. Am.* **86**, 1255–1269.
- Randall, G. R., C. J. Ammon, and T. J. Owens (1994). Moment-tensor estimation using regional seismograms from a Tibetan Plateau portable network deployment, *Geophys. Res. Lett.* **22**, 1665–1668.
- Romanowicz, B., D. Dreger, M. Pasyanos, and R. Uhrhammer (1993). Monitoring of strain release in central and northern California using broadband data, *Geophys. Res. Lett.* **20**, 1643–1646.
- Rueda, J., and J. Mezcua (2005). Near-real-time seismic moment-tensor determination in Spain, *Seism. Res. Lett.* **76**, 455–465.
- Saikia, C. K. (1994). Modified frequency-wavenumber algorithm for regional seismograms using Filon’s quadrature: modeling of L_g waves in eastern North America, *Geophys. J. Int.* **118**, 142–158.
- Sipkin, S. A. (1982). Estimation of earthquake source parameters by the inversion of wave-form data: synthetic waveforms, *Phys. Earth Planet. Interiors* **30**, 242–259.
- Sipkin, S. A. (1994). Rapid determination of global moment-tensor solutions, *Geophys. Res. Lett.* **21**, no. 16, 1667–1670.
- Thio, H. K., and H. Kanamori (1995). Moment tensor inversions for local earthquakes using surface waves recorded at TERRAScope, *Bull. Seism. Soc. Am.* **85**, 1021–1038.
- Wessel, P., and W. H. F. Smith (1998). New, improved version of Generic Mapping Tools released, *EOS Trans. AGU* **79**, no. 47, 579.
- Zhu, L., and D. V. Helmberger (1996). Advancement in source estimation techniques using broadband regional seismograms, *Bull. Seism. Soc. Am.* **86**, no. 5, 1634–1641.

Seismological Laboratory
 Division of Geological and Planetary Sciences
 California Institute of Technology
 Pasadena, California 91125
 hauksson@gps.caltech.edu
 solanki@gps.caltech.edu

Manuscript received 2 December 2005.